The Arabidopsis Framework Model version 2 predicts the organism-level effects of circadian clock gene mis-regulation

in silico Plants Vol. 4, No. 2, pp. 1–15
https://doi.org/10.1093/insilicoplants/diac010
Advance Access publication 30 May 2022
Special Issue: Integrative and Multiscale Modelling
Original Research

in silico Plants
OXFORD

The *Arabidopsis* Framework Model version 2 predicts the organism-level effects of circadian clock gene mis-regulation

Yin Hoon Chew[1,7], Daniel D. Seaton[1,8], Virginie Mengin[2,9], Anna Flis[2], Sam T. Mugford[3], Gavin M. George[4,10], Michael Moulin[5,11], Alastair Hume[6], Samuel C. Zeeman[4], Teresa B. Fitzpatrick[5], Alison M. Smith[3], Mark Stitt[2] and Andrew J. Millar*[,1]

[1]SynthSys and School of Biological Sciences, C. H. Waddington Building, University of Edinburgh, King's Buildings, Edinburgh EH9 3BF, UK
[2]Max Planck Institute of Molecular Plant Physiology, Am Muehlenberg 1, 14476 Potsdam-Golm, Germany
[3]Department of Metabolic Biology, John Innes Centre, Norwich NR4 7UH, UK
[4]Institute of Molecular Plant Biology, ETH, Zurich, Switzerland
[5]Department of Botany and Plant Biology, University of Geneva, Geneva, Switzerland
[6]SynthSys and EPCC, Bayes Centre, University of Edinburgh, 47 Potterrow, Edinburgh EH8 9BT, UK
[7]Present address: School of Mathematics, Watson Building, University of Birmingham, Birmingham B15 2TT, UK
[8]Present address: GSK, Gunnels Wood Road, Stevenage, Hertfordshire SG1 2NY, UK
[9]Present address: School of Life Sciences, University of Essex, Wivenhoe Park, Colchester CO4 3SQ, UK
[10]Present address: Puregene AG, Etzmatt 273, CH-4314 Zeiningen, Switzerland
[11]Present address: Département de Médecine (DM) et de Médecine de Laboratoire et Pathologie, Centre Hospitalier Universitaire Vaudois (CHUV), Lausanne, Switzerland
*Corresponding author's e-mail address: Andrew.Millar@ed.ac.uk

Handling Editor: Amy Marshall-Colon

Citation: Chew YH, Seaton DD, Mengin V, Flis A, Mugford ST, George GM, Moulin M, Hume A, Zeeman SC, Fitzpatrick TB, Smith AM, Stitt M, Millar AJ. 2022. The *Arabidopsis* Framework Model version 2 predicts the organism-level effects of circadian clock gene mis-regulation. *In Silico Plants* **2022**: diac010; doi: 10.1093/insilicoplants/diac010

ABSTRACT

Predicting a multicellular organism's phenotype quantitatively from its genotype is challenging, as genetic effects must propagate across scales. Circadian clocks are intracellular regulators that control temporal gene expression patterns and hence metabolism, physiology and behaviour. Here we explain and predict canonical phenotypes of circadian timing in a multicellular, model organism. We used diverse metabolic and physiological data to combine and extend mathematical models of rhythmic gene expression, photoperiod-dependent flowering, elongation growth and starch metabolism within a Framework Model for the vegetative growth of *Arabidopsis thaliana*, sharing the model and data files in a structured, public resource. The calibrated model predicted the effect of altered circadian timing upon each particular phenotype in clock-mutant plants under standard laboratory conditions. Altered night-time metabolism of stored starch accounted for most of the decrease in whole-plant biomass, as previously proposed. Mobilization of a secondary store of malate and fumarate was also mis-regulated, accounting for any remaining biomass defect. The three candidate mechanisms tested did not explain this organic acid accumulation. Our results link genotype through specific processes to higher-level phenotypes, formalizing our understanding of a subtle, pleiotropic syndrome at the whole-organism level, and validating the systems approach to understand complex traits starting from intracellular circuits.

KEYWORDS: Data sharing; gene regulatory network; genotype to phenotype; mathematical model; metabolism; open research; photosynthesis.

1. INTRODUCTION

Circadian clocks in all organisms integrate multiple environmental inputs and affect disparate, potentially interacting biological processes, from sleep/wake cycles in mammals to flowering in plants (Kuhlman *et al.* 2018). Clock genes are rarely essential but appropriate alleles can confer an organismal growth (Green *et al.* 2002) and competitive advantage (Ouyang *et al.* 1998; Dodd *et al.* 2005) and have been repeatedly selected during crop domestication (Bendix *et al.* 2015; Muller *et al.* 2015). Mis-timed mutant organisms suffer a syndrome of mild, environment-dependent effects akin to a chronic disease (Dodd *et al.* 2005; Paschos *et al.* 2010; Peek *et al.* 2013), including traits that are not overtly related to rhythmicity. Small networks of 'clock genes' drive these 24-h, biological rhythms in eukaryotes (Millar 2016; Kuhlman *et al.* 2018). A few among thousands of downstream, clock-regulated genes are known to mediate physiological phenotypes, such as the metabolic syndrome of clock-mutant animals (Peek *et al.* 2013). However, identifying such causal links along biosynthetic, signalling or developmental pathways is not sufficient to predict quantitatively the whole-organism phenotypes due to circadian mis-timing: formal, mathematical models are required.

Predictive modelling from cellular mechanisms in multicellular organisms has best succeeded for phenotypes that closely map the behaviour of gene circuits (von Dassow *et al.* 2000) or signalling pathways (Band *et al.* 2014). From the whole-organism perspective, these cases can be described as having a 'short phenotypic distance' from the genotype (Hammer *et al.* 2019). However, a recent review (Clark *et al.* 2020) points out that whole-plant models that link to the molecular level 'are rare' (Grafahrend-Belau *et al.* 2013; Chew *et al.* 2014), despite the long-standing aspiration to understand and manipulate the field-scale traits that distinguish crop varieties based on their underlying genetic differences (Hammer *et al.* 2019; Matthews and Marshall-Colon 2021), and the potential applications in breeding programmes or studies of natural selection. Here, we extend one of the rare, whole-plant models to understand the pleiotropic phenotypes controlled by the circadian clock.

The *Arabidopsis* Framework Model version 1 (FMv1) represents the interacting, physiological components of vegetative growth in *Arabidopsis thaliana* up to flowering, in a simple, modular fashion (Chew *et al.* 2014). The model was designed to study circadian effects on physiology but has proved more broadly useful (Matthews and Marshall-Colon 2021), as evidenced by the re-use and adaptation of FMv1 to understand the effects of gibberellin (GA)-related regulatory proteins on biomass and leaf architecture (Pullen *et al.* 2019), of temperature on flowering via *FT* gene regulation and/or leaf development (in FMv1.5; Kinmonth-Schultz *et al.* 2019) and of phytochrome-regulated cotyledon size upon adult plant biomass (Krahmer *et al.* 2021). A simplified version of FMv1 (FM-lite) was included in a whole-lifecycle model of *Arabidopsis* (FM-life) to test the adaptive value of phenology traits (Zardilis *et al.* 2019). We now update FMv1 with biochemically detailed submodels of the circadian clock and of its outputs, and a revised allocation of photosynthetic carbon with a circadian input.

The *Arabidopsis* clock mechanism comprises dawn-expressed transcription factors *LATE ELONGATED HYPOCOTYL* (*LHY*) and *CIRCADIAN CLOCK-ASSOCIATED 1* (*CCA1*), which inhibit the expression of evening genes such as *GIGANTEA* (*GI*), as illustrated by their respective RNA expression profiles in plants grown under light:dark cycles (Fig. 1A; Flis *et al.* 2015). *LHY* and *CCA1* expression is inhibited by PSEUDO-RESPONSE REGULATOR (PRR) proteins. Removing the earliest-expressed *PRR* genes in *prr7prr9* mutants slows the clock (Nakamichi *et al.* 2010), because *LHY* and *CCA1* expression is not inhibited as quickly as in wild-type plants. Under constant light, rhythmic outputs have a circadian period around 30 h in the double-mutant plants, compared to 24.5 h in the wild type (Salome and McClung 2005). The decline of *LHY* and *CCA1* RNA levels in the double mutants is delayed under light:dark cycles, as is the subsequent rise of *GI* and other target genes (Fig. 1B). A series of mathematical models has represented the increasingly detailed biochemistry of the clock gene circuit (Pokhilko *et al.* 2012; Fogelmark and Troein 2014; Urquiza-García and Millar 2021), recapitulating the effects of the *prr7prr9* mutations on clock gene dynamics (Fig. 1A and B; Pokhilko *et al.* 2012; Flis *et al.* 2015). Our focus here is not on the clock's mechanism but on its effects.

The clock models have been extended to the output pathways that convey circadian timing information to control downstream processes, starting with the control of flowering time in response to photoperiod (Welch *et al.* 2005; Salazar *et al.* 2009). The light-responsive pathways of gene regulation that control both flowering and organ elongation have been modelled with increasing biochemical detail (Seaton *et al.* 2015) or more simply (De Caluwé *et al.* 2016; Pay *et al.* 2022), while other models have represented the non-circadian inputs that also control flowering (Wilczek *et al.* 2009; Chew *et al.* 2012). The first representations of circadian metabolic outputs have focussed on the nightly, clock-limited rate of sugar mobilization from storage in transient starch (Graf *et al.* 2010). Starch receives the largest portion of photosynthate in *Arabidopsis* leaves, after sugars, and clock regulation ensures that leaves use as much of each day's carbon store for night-time growth as possible, leaving just 2–5 % at dawn (Smith and Zeeman 2020). Models of this process have focussed variously on the biochemistry of the regulated degradation, its connection to the clock mechanism, or the potential impact of the resulting sugar on clock dynamics (Scialdone *et al.* 2013; Pokhilko *et al.* 2014; Seaton *et al.* 2014; Seki *et al.* 2017), but without considering the resulting growth of the plant. We therefore tested whether these proposed mechanisms were sufficient to understand the multiple phenotypes of the long-period clock-mutant *prr7prr9*, not only for the photoperiodic regulation of flowering, which is arguably a short phenotypic distance from the clock genes, but also the more distant biomass growth and metabolic traits.

2. METHODS

2.1 Experimental methods

2.1.1 Plant materials and growth conditions. *Arabidopsis thaliana* of the Columbia (Col-0) accession, *prr7-3/prr9-1* (Nakamichi *et al.* 2007) and *lsf1-1* (Comparot-Moss *et al.* 2010) were used in this study. Seeds were first sown on half strength Murashige and Skoog (MS) solution and stratified in darkness at 4 °C for 5 days before being exposed to white light at the desired photoperiod and temperature. Four-day-old seedlings were then transferred to soil containing Levington seed and modular compost (plus sand). The growth and treatment conditions

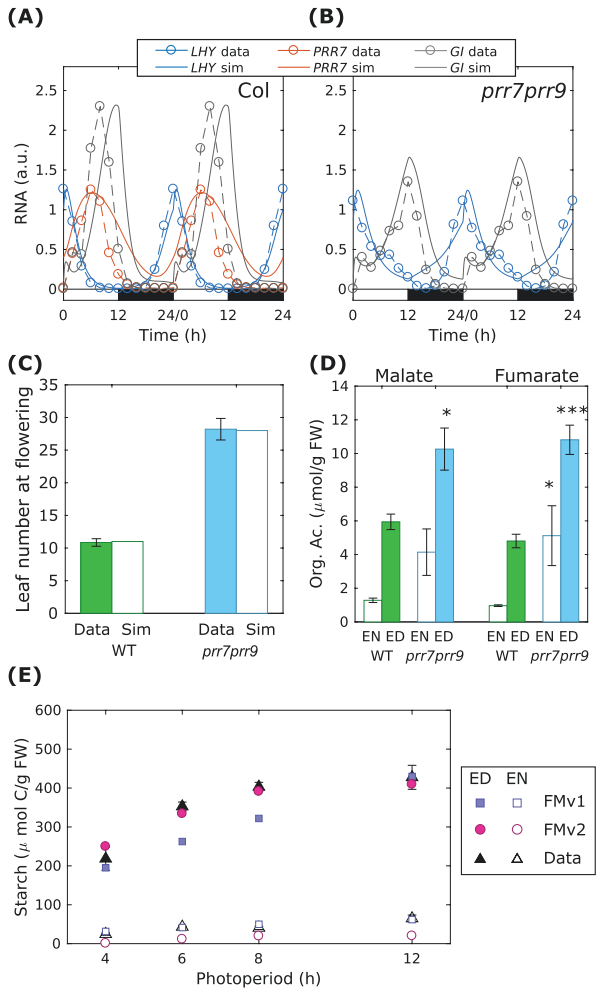

Figure 1. Simulation of clock dynamics and clock outputs. (A, B) Clock gene mRNA abundance (Flis *et al.* 2015) for wild-type (Col) and *prr7prr9* plants (dashed lines, symbols), and FMv2 simulations (solid lines), under 12-h light:12-h dark cycles (12L:12D), double-plotted, normalized to Col level. (C) Rosette leaf number at flowering (Nakamichi *et al.* 2007) under 16L:8D (filled), compared to simulation (open). (D) Malate and fumarate accumulation (mean ± SEM, $n = 4$) in Col and *prr7prr9* at end of day (ED) or night (EN) under 12L:12D, 20 °C, light intensity = 160 μmol m^{-2} s^{-1}; *t*-tests compared *prr7prr9* to Col (*$P < 0.05$; ***$P < 0.001$); *prr7prr9* EN $n = 3$. (E) Starch levels at ED (filled) and EN (open) after 30 days under various photoperiods (Sulpice *et al.* 2014) (triangles), compared to FMv1 (squares), FMv2 (circles).

for each experiment are shown in the figure legends. For the experiment in Fig. 1D and **Supporting Information—Fig. S3** only, seeds were sown on wet soil in pots and transferred directly to experimental conditions. Plants were thinned after a week and treated with nematodes after two weeks as a biological pest control.

2.1.2 Leaf number and plant assay. The total number of leaves (including the cotyledons) was recorded every 3–4 days from seedling emergence. Only leaves exceeding 1 mm^2 in size (by eye) were considered in the total leaf count. Plants were harvested for biomass at different time points and for metabolite measurement at 3 weeks [**see Supporting Information—Fig. S3**] and 4 weeks (other data). For metabolite measurement, rosettes were harvested and immediately submerged in liquid nitrogen, half an hour before lights-off (end of day, ED) or lights-on (end of night, EN) and stored at −80 °C until extraction. For dry biomass, dissected plants were oven-dried at 80 °C for 7 days. Area analysis was conducted using ImageJ (Schneider *et al.* 2012). Each image was first processed with colour thresholding to isolate the green region, which was next converted into binary format. The area was then determined using the Analyze Particles tool.

2.1.3 Gas exchange measurement. An EGM-4 Environmental Gas Monitor for CO_2 (PP Systems, USA) was used for CO_2 flux measurement. A Plexiglass cylindrical chamber (12 cm in diameter × 3 cm sealed height, with a 6-cm tall support) was used [**see Supporting Information—Fig. S5F**]. Rubber rings around the lid and the hole for the pot ensured an airtight seal. The chamber was connected to the EGM-4 with two butyl tubes for closed-loop measurement.

Each individual measurement was taken by placing an individual plant pot in the chamber for approximately 60 s, during which the EGM-4 recorded CO_2 concentration (μmol mol^{-1} or ppm) every 4.6 s. We covered the soil surface of the pots with black opaque plastic, leaving only a small hole in the middle for the plants. Plants were measured when they were 37 days old. Dark respiration was measured one hour before lights-on while daytime assimilation was measured one hour before lights-off.

CO_2 enrichment of the atmosphere in the growth chambers due to the experimenters' breathing was avoided by using a breath-scrubbing device during measurement. Hourly CO_2 concentration at leaf level was also monitored by connecting the EGM-4 to a computer for automated data logging. The average hourly CO_2 level was used as input to the model.

2.1.4 Extraction and determination of metabolite content. Rosettes were harvested as described above and ground in liquid nitrogen. Key results for 28-day-old plants are presented here; further results from the same experiments are available in the shared data files (see below). Around 20 mg of ground material was aliquoted in screw-cap tubes (Micronic). Ethanolic extraction was performed using 80 % ethanol (v/v) with 10 mM 2-(N-morpholino)ethanesulfonic acid (MES) (pH 5.9) and 50 % ethanol (v/v) with 10 mM MES (pH 5.9). During extraction, the successive supernatants obtained were combined into 96-deep well plates. The supernatant was used for spectrophotometric determination of chlorophylls, soluble carbohydrates, amino acids and organic acids as described (Arrivault *et al.* 2009). The pellet remaining after the ethanolic extraction was used for the determination of starch and total protein content as described (Pyl *et al.* 2012).

For **Supporting Information—Fig. S10A–C**, phosphoenolpyruvate carboxylase (PEPC) activity and incorporation of labelled $^{14}CO_2$ into metabolite pools was measured as previously described for whole-plant labelling (Kölling *et al.* 2013, 2015) with minor modifications. Near the end of the night (ZT20-21), 28-day-old plants were transferred to a custom built, sealed chamber in the

dark. Each replicate consisted of the aerial parts of a single plant. Labelling was initiated through the release of $^{14}CO_2$ (150 μCi) from $NaH^{14}CO_3$ with the addition of lactic acid. After 1 h, the plants were harvested into 5 mL 80 % (v/v) ethanol and incubated for 15 min at 80 °C. Following homogenization, the soluble fraction was collected by centrifugation (2400*g*, 12 min), pooled with four sequential 1-mL washes (50 % ethanol, 20 % ethanol, water and then 80 % ethanol) of the insoluble fraction pellet. The soluble fraction was concentrated under vacuum. A water-soluble subfraction was collected by dissolving the near-dry exsiccate in 2 mL water, while the remainder was dissolved in 2 mL 98 % ethanol. Basic, acidic and neutral fractions were separated from the water-soluble fraction by ion-exchange chromatography as described (Quick *et al.* 1989). Partitioning into protein was measured as described (Kölling *et al.* 2013). Isotope incorporation into each fraction was measured by liquid scintillation counting.

For **Supporting Information Fig. S10D–F**, the extraction of B1 vitamers was performed using 100 mg of plant tissue homogenized in 200 μL of 1 % (v/v) trichloroacetic acid. The mixture was centrifuged for 10 min at 10 000*g* and the supernatant decanted. B1 vitamers were derivatized and quantified by a high-performance liquid chromatography method as described (Moulin *et al.* 2013). The data were normalized to the tissue fresh weight.

2.2 Modelling methods

Development of the FMv2 in Matlab (Mathworks, Cambridge, UK), model equations, experimental data for model calibration and simulation procedures are described in **Supporting Information—Methods** section.

3. RESULTS

3.1 Circadian control of plant development

The FMv1 was designed with a modular structure, which facilitated our replacement of the earlier clock and photoperiod pathway submodel (Salazar *et al.* 2009) with more detailed submodels (Pokhilko *et al.* 2012; Seaton *et al.* 2015) that explicitly represent the clock genes *PRR7*, *PRR9* and output pathway genes [**see Supporting Information—Section 1**]. Table 1 summarizes the changes in the submodels of the *Arabidopsis* Framework Model version 2 (FMv2) compared to FMv1, and notes the abbreviated names for the clock (P2011), starch (S2014) and photoperiodism (S2015) submodels. Figure 2 shows the updated gene circuits in the context of the Framework Model's other functions.

Flowering time in *Arabidopsis* is commonly scored by the number of rosette leaves produced before the flowering bolt elongates above the vegetative rosette, under long and short photoperiods. Predicting leaf number involves the FM's clock and photoperiod (Seaton *et al.* 2015), phenology (Chew *et al.* 2012) and functional–structural submodels (Christophe *et al.* 2008), suggesting that this phenotype can only be considered a 'short distance' from the clock genes in the sense that it does not involve the metabolic submodel. The P2011 clock submodel (Pokhilko *et al.* 2012) was known to recapitulate the altered clock gene expression dynamics in *prr7prr9* double-mutant plants in general. Figure 1A and B show that simulations of the published model also closely matched the later, reference data set of RNA time series from the TiMet project (Flis *et al.* 2015) in the double mutants. In brief, the late circadian phase in the mutant simulation reduces the *FT* mRNA output from the S2015 submodel (**see Supporting Information—Section 1**; Fig. 2). The phenology model therefore takes longer to reach the abstract photothermal threshold for flowering, giving more time for the functional–structural model to produce rosette leaves.

The new model combination in the FMv2 matched the leaf number data published by the Mizuno group (Nakamichi *et al.* 2007) for wild-type Columbia (Col) plants under long photoperiod growth conditions (Fig. 1C). The expectation from FMv1 was that calibration of the photothermal time threshold for flowering (Fig. 2) might often be required for the model to match the absolute leaf numbers observed across different laboratories (Chew *et al.* 2014) but that calibration was not required in this case. The late circadian phase predicted a lower activation of the photoperiod response mechanism and predicted a late-flowering phenotype in the *prr7prr9* mutants in these conditions, which was also exactly matched by the model (Fig. 1C). Under short photoperiods, wild-type plants flower late and the clock-dependent, photoperiodic pathway has little effect. It is therefore expected that the double mutant's flowering time is closer to the wild type, as observed in the data and qualitatively in the simulations [**see Supporting Information—Fig. S1A**]. The model predicted slightly later flowering than was observed in both genotypes, however, suggestive of a non-photoperiodic effect on flowering.

The S2015 submodel further predicts the regulation of elongation growth in the seedling hypocotyl, which is light- and therefore photoperiod-dependent. The FMv2 matched the observed photoperiodic regulation of hypocotyl elongation in wild-type plants, in data again from the Mizuno group (Niwa *et al.* 2009). The longer hypocotyls of *prr7prr9* seedlings were qualitatively matched by the model [**see Supporting Information—Fig. S1B**], with an altered balance between long and short photoperiods that suggests further, secondary mechanism(s) may be involved, and comparison to later models could be informative (De Caluwé *et al.* 2016).

3.2 Mis-regulation of carbon dynamics

In contrast to the rapid, finite elongation of the seedling hypocotyl, long-term biomass growth of the whole plant is mediated by the metabolic network, the development of sink and source organs and the partitioning of metabolic resources amongst them. Among many potential circadian effects on metabolism, we focus on the clock-limited rate of sugar mobilization from starch. First, we addressed an observed limitation of the starch dynamics in the metabolic submodel of the FMv1. Daytime starch accumulation in wild-type plants was underestimated by the model under short photoperiods (Chew *et al.* 2014; Sulpice *et al.* 2014), indicating that the 'growth-first' control of photoassimilate partitioning in FMv1 should be updated. Instead of an 'overflow' to starch after growth demand was satisfied, FMv2 uses photoperiod-dependent, 'starch-first' partitioning. The key, starch biosynthetic enzyme, AGPase, was clearly photoperiod-dependent at the level of measured activity (**see Supporting Information—Fig. S2A**; Mugford *et al.* 2014), and in the abundance of some protein subunits (Seaton *et al.* 2018). The measured photoperiod control of AGPase activity was therefore introduced into the model as a candidate mechanism for this photoperiod-dependent partitioning [**see Supporting Information—Section 2**]. This change

Table 1. Changes to the submodels and processes of the FMv2 compared to the FMv1. The origins of the multiple submodels that were combined to form the FMv1 are noted, together with the origins of the updated submodels and other components of the FMv2.

Model function	Process	In FMv1	Derived from	In FMv2	Submodel	Derived from
Environmental data input	Hourly light intensity, $[CO_2]$, temperature, sunrise/sunset times		–	As in FMv1		
Functional–structural plant model	Organ sink demand	Thermal time function	Christophe *et al.* (2008)	As in FMv1		
	Leaf initiation	Stochastic function	–	As in FMv1		
	Shoot/root allocation	Emergent behaviour	–	As in FMv1		
Carbon dynamic model	Photosynthate partitioning	'Basal + Overflow'	Rasse and Tocquin (2006)	'Starch-first', using AGPase data	–	This work
	Starch mobilization	Fixed rate	Rasse and Tocquin (2006)	Controlled by P2011 clock model	From S2014 Model 2	Seaton *et al.* (2014)
	Malate and fumarate pool	–	–	New model component	–	This work
Circadian clock model	Light-entrained rhythms	4 RNAs, 4 proteins, 0 protein complexes; lacks *PRR7, PRR9*	Locke *et al.* (2005)	9 RNAs, 16 proteins, 6 protein complexes; includes *PRR7, PRR9*	P2011	Pokhilko *et al.* (2012)
Photoperiodism model	External coincidence detector	1 RNA, 1 protein	Salazar *et al.* (2009)	4 RNAs, 3 proteins	S2015	Seaton *et al.* (2015)
Light signalling model	Phytochrome/phytochrome-interacting factor (PIF) pathway	–	–	4 RNAs, 3 proteins	S2015	Seaton *et al.* (2015)
Phenology model	Seedling emergence, flowering time	Diel photothermal time	Chew *et al.* (2012)	As in FMv1		

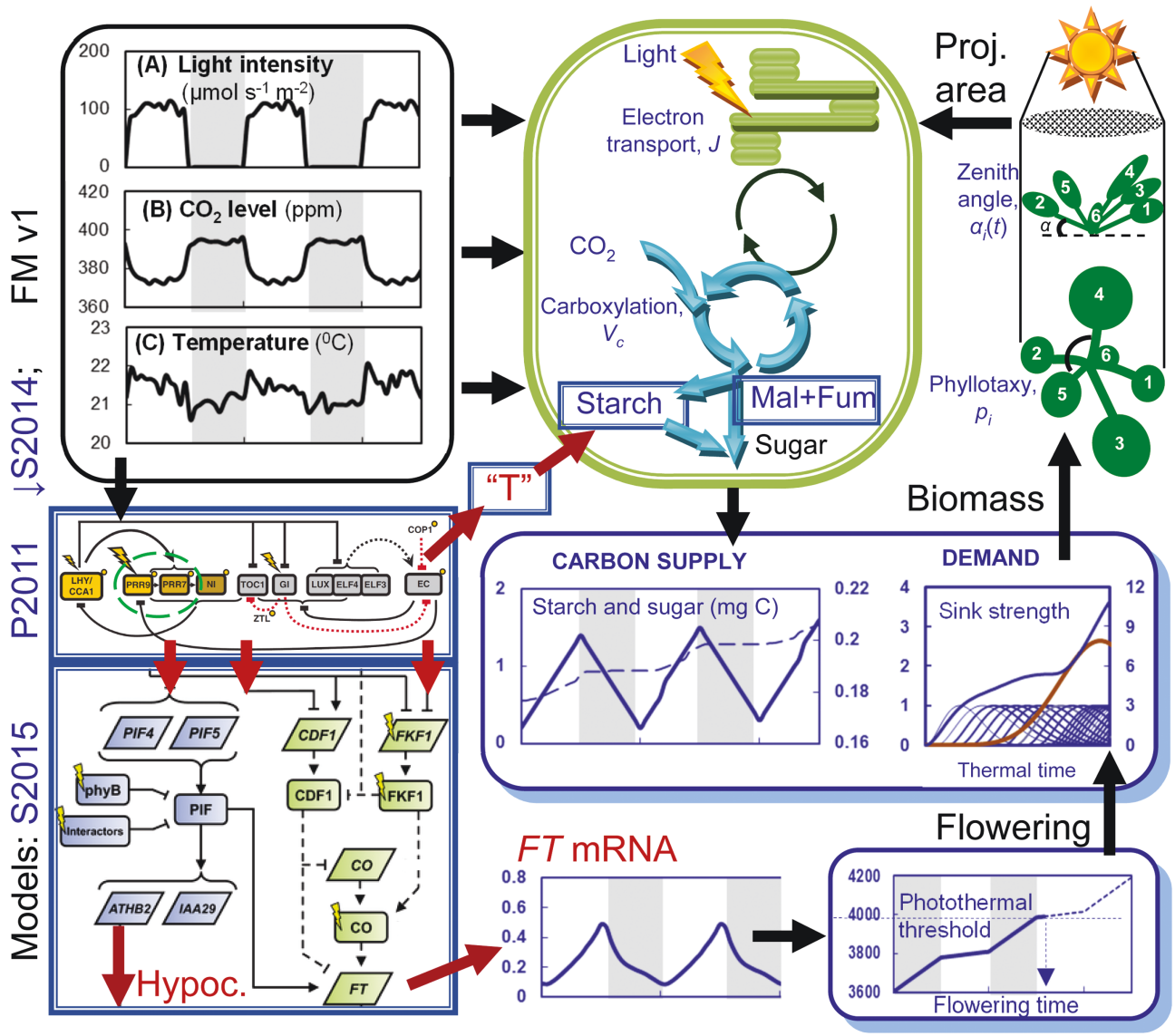

Figure 2. Operation of the *Arabidopsis* Framework Model version 2 (FMv2). Model components that are updated in FMv2 are bounded in double rectangles, with abbreviated model names (left). Key outputs from the new models are shown as arrows leaving the bounding rectangles. The P2011 clock model shows only clock genes for clarity. Morning or day genes, yellow symbols; evening genes and the evening complex (EC), grey symbols. The PRR9 and PRR7 genes that are inactivated in the prr7prr9 double mutant are marked with a dashed oval. Components of P2011 drive the S2014 starch degradation model via component 'T' (centre), and the S2015 external coincidence model (lower left). S2015 controls photoperiod-dependent hypocotyl elongation (Hypoc.) by rhythmically gating the PhyB/PIF/ATHB2 pathway, and the florigen FT by the CDF1/FKF1/CO pathway. The S2015 cartoon distinguishes RNA components (paralellograms) from proteins (rounded rectangles). Light inputs are shown as flashes. Among the model components retained from the FMv1, the carbon dynamic model (bounded in green) includes updated starch and malate and fumarate (Mal + Fum) carbon stores, and provides Sugar as the Carbon Supply for growth. This is allocated according to the Demand of leaf (blue) and root (red) sinks in the functional–structural plant model, which uses the leaf Biomass to calculate the rosette's projected area for photosynthesis (Proj. area). When the Photothermal model (lower right) reaches the threshold for Flowering, the simulation ends.

partitioned sufficient carbon to starch in simulated, short photoperiods to match the experimental data in photoperiods of up to 12 h [**see Supporting Information—Fig. S2A**]. Under longer photoperiods, *Arabidopsis* plants manage the greater photosynthate supply using additional metabolic and physiological regulation that is not represented in the FMv2 (Sulpice *et al.* 2014; Ishihara *et al.* 2022).

At night, starch is mobilized (degraded) at a constant rate to provide sugar until dawn, as anticipated by the circadian clock

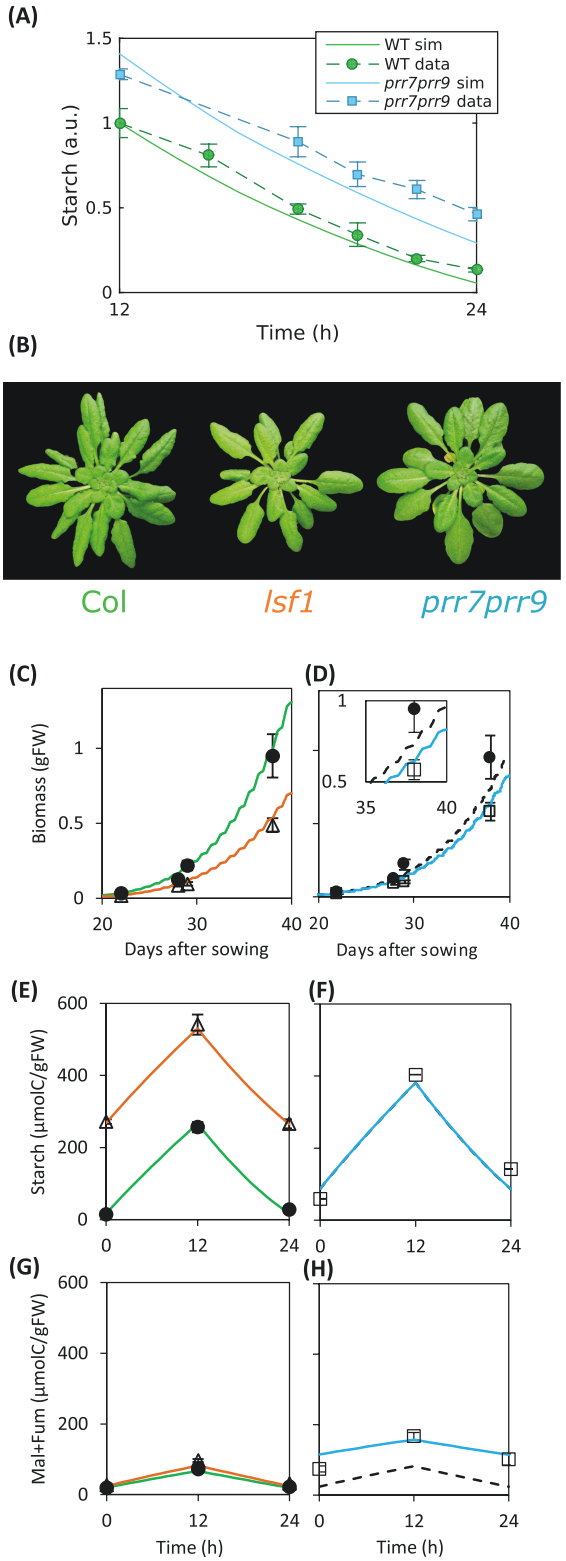

Figure 3. Contributions of starch and organic acids to biomass growth. (A) *prr7prr9* plants (blue, squares) have higher starch levels than Col (WT, green, circles), mean ± SEM, *n* = 6, similar to the starch accumulation due to the slower relative starch degradation rate in simulations of the FMv2 where *PRR7* and *PRR9* are mutated (solid lines). Data and model normalized to Col at 12 h. (B) Thirty-eight-day-old Col, *lsf1*, *prr7prr9* plants. (C–H) Data (symbols) and simulation (lines) of fresh weight (C, D), starch (E, F) and total malate and fumarate (G, H) for Col (circles, green), *lsf1* (triangles, orange) and *prr7prr9* plants (squares). Simulations of *prr7prr9* show a starch defect only (dashed black line) or both starch and malate + fumarate defects (solid blue). (D) Inset enlarges main panel around 38-day data point. Data show mean ± SD; *n* = 5 for biomass; *n* = 3 for metabolites, where each sample pooled three plants. Growth conditions, 12L:12D with light intensity = 190 µmol m^{-2} s^{-1} (A) or 145 µmol m^{-2} s^{-1} (B–H), temperature 20 °C (A), 20.5 °C (B–H); CO_2 = 420 ppm.

(Graf *et al.* 2010; Scialdone *et al.* 2013). We therefore included the starch degradation mechanism from a further, published submodel (S2014) that links starch degradation to the clock submodel, and had been shown to match the early depletion of starch reserves in mutant plants with a short circadian period and in other, discriminating conditions (Seaton *et al.* 2014; **see Supporting Information—Section 1**). Simulation of the revised model closely matched the starch levels of wild-type plants under photoperiods of up to 12 h (Fig. 1E). Finally, the organic acids malate and fumarate also accumulate significantly during the day in *Arabidopsis*, are mobilized at night and have been proposed as secondary carbon stores (Zell *et al.* 2010). Analysis of 22 further metabolites revealed that at the end of the day, levels of malate and fumarate were 2-fold higher in *prr7prr9* mutants than wild type, with a lesser elevation in citrate and in the much smaller pools of aconitate and isocitrate (Fig. 1D; **see Supporting Information—Fig. S3**). The malate and fumarate pools were also increased at night in the mutants, albeit with greater variability, so these were prioritized for further analysis in the double mutants, alongside starch. As a simple approximation, the sum of malate and fumarate was included as an 'organic acid' pool with dynamics similar to starch, in the FMv2 (**see Supporting Information—Section 3**; Fig. 2). If altered starch mobilization in the long-period clock-mutant *prr7prr9* was sufficient to affect its biomass, then the FMv2 should also predict that phenotype.

3.3 Control of biomass *via* starch degradation

We first tested whether the FMv2 could explain the biomass phenotype caused by a mild, direct change in starch degradation, in mutants of *LIKE SEX FOUR 1* (*LSF1*) that were tested for 12 major metabolite pools (Arrivault *et al.* 2009; Pyl *et al.* 2012) and the physiological parameters required to calibrate the FMv2. *LSF1* encodes a phosphatase homologue located in the chloroplast, which interacts with β-amylases and is necessary for normal starch mobilization (Comparot-Moss *et al.* 2010; Schreier *et al.* 2019). *lsf1* mutants grown under 12L:12D have mildly elevated starch levels and reduced biomass, similar to the *prr7prr9* clock mutant (Fig. 3B, C and E). Reducing the relative starch degradation rate in the FMv2 [**see Supporting Information—Table S1**] recapitulated the higher levels of starch in *lsf1* that were observed in published studies (Comparot-Moss *et al.* 2010; **see Supporting Information—Fig. S1C**) and in new data (Fig. 3E). To reproduce the biomass growth of wild-type plants, a minimal model

calibration workflow [**see Supporting Information—Fig. S4**] used measured photosynthetic and metabolic variables [**see Supporting Information—Fig. S5**] to calibrate the model for our conditions [**see Supporting Information—Table S1**]. The water content was previously highlighted as a key parameter; by setting its value to the mean water content observed for each genotype, model predictions can be compared to fresh weight data (Chew *et al.* 2014). Introducing a lower starch degradation rate, to reproduce the higher starch levels observed in *lsf1*, and its measured water content into the calibrated model accurately predicted the reduced biomass of *lsf1* mutant plants (Fig. 3C). The coefficient of variation of the Root-Mean-Square Error (cvRMSE) provides a normalized error metric for all biomass data (Chew *et al.* 2014), showing a good fit to both *lsf1* and wild-type genotypes (8.0 % Col and 13.7 % *lsf1*), and validating the FMv2 for biomass prediction. In addition to the direct prediction of carbon biomass, the FMv2 predicts the gain of other major biomass components indirectly, allowing further validation. The change in biomass gain from day to night in simulated, wild-type plants predicted a 3.3-fold increase in protein synthesis rates in daytime, compared to night-time, for example. This was very close to the observed 3.1-fold increase in protein synthesis in published data (Ishihara *et al.* 2015; **see Supporting Information—Section 5**).

3.4 Control of biomass in the circadian clock mutant

prr7prr9 mutants showed higher starch levels at both dawn and dusk than the wild type (Fig. 3A; **see Supporting Information—Fig. S1D**), indicative of a slower relative starch degradation rate, similarly to the *lsf1* mutants (see Discussion section). The starch profiles of plants grown in Norwich (Fig. 3A; **see Supporting Information—Fig. S1D**) and in Edinburgh (Fig. 3F) closely matched the profiles predicted by simulating *prr7prr9* mutations in the clock submodel of the FMv2. The biomass of *prr7prr9* mutant plants was 40 % lower than wild-type control plants at 38 days. The calibrated FMv2 also predicted a lower biomass in *prr7prr9* due to the starch defect but with a smaller effect than in the data (26 % biomass reduction). A poor model fit (cvRMSE = 41 %) indicated that process(es) additional to starch degradation were likely to account for the limited growth of *prr7prr9* but not of *lsf1* plants in this study. *prr7* single mutants fully mobilized starch and grew normally, as predicted from their normal circadian timing [**see Supporting Information—Fig. S6**]. The mild starch excess at the end of the day aligns with past reports (Haydon *et al.* 2013; Seki *et al.* 2017) but apparently had no effect on biomass growth in *prr7* plants. We therefore sought another clock-regulated process that might contribute to reduce the biomass of *prr7prr9* plants.

Model calibration data showed that photosynthesis, starch synthesis and leaf production rates were unaffected by the *prr7prr9* mutations [**see Supporting Information—Fig. S5**]. Water content was slightly reduced in *prr7prr9* [**see Supporting Information—Table S1**] and this is the most sensitive parameter in our model [**see Supporting Information—Fig. S7**]. However, neither 1 SD variation in the mutant's simulated water content, nor any measured water content value allowed the model with only the clock (and hence starch) defect to match the mutant biomass [**see Supporting Information—Fig. S8**].

Considering the pool of malate and fumarate as a secondary carbon store (Zell *et al.* 2010), the amount of carbon mobilized from malate and fumarate at night in the wild type was up to 19 % of the carbon mobilized from starch. *prr7prr9* but not *lsf1* plants accumulated excess malate and fumarate, representing further 'wasted' carbon that did not contribute to biomass growth (Fig. 3G and H), consistent with independent sampling of this double mutant (Flis *et al.* 2019). We therefore reduced the relative malate and fumarate mobilization rate in the FMv2 simulation of *prr7prr9*, to reproduce the observed organic acid excess (Fig. 3H). Together, the simulated defects in starch and organic acid mobilization quantitatively accounted for the mutant's reduced biomass (Fig. 3D; cvRMSE = 15.1 %).

3.5 Replication of the physiological phenotypes

The *prr7prr9* double mutants showed the phenotypes noted above in three further experiments (Fig. 4). The final biomass of the double mutants ranged from 53 to 76 % of the wild-type value, compared to a mean of 60 % in Experiment 1 (Fig. 3). Calibrating the models with measured physiological parameters facilitated the comparison among these studies [**see Supporting Information—Section 4**]. The biomass of the double mutants in Experiment 2 was also below the biomass predicted from slower starch degradation rate alone [**see Supporting Information—Fig. S9G**]. As in Experiment 1, the photoassimilate retained in the mutant's starch, malate and fumarate pools together accounted for its lower biomass in Experiment 2. Both wild-type and clock-mutant genotypes grew slightly larger in Experiment 3 than the model simulations predicted [**see Supporting Information—Fig. S9A**]. Photosynthetic rates measured at a single time point might not have adequately calibrated the model in this case to simulate growth over several weeks. The mutant's starch degradation rate matched the FMv2 prediction in Experiment 3 and the consequent, clock-dependent effect on starch degradation alone in the simulations sufficiently accounted for the mutants' biomass (72 % of wild-type biomass, cvRMSE 4.4 %). Reducing the simulated mobilization of the malate and fumarate pool, as in the simulations of Experiments 1 and 2, slightly underestimated the mutants' biomass in Experiment 3 (**see Supporting Information—Fig. S9A**; cvRMSE 12.1 %). The Col and *prr7prr9* control plants in an experiment on GA effects (see below) again replicated these phenotypes ('no GA', Fig. 4; **see Supporting Information—Fig. S9**). The GA study was not designed to collect full calibration data, so simulations were not performed.

Experiment 2 showed slower biomass growth, and the smallest effects of the *prr7prr9* mutation on several phenotypes (Fig. 4; **see Supporting Information—Fig. S9**). Mutant plants retained mean starch levels over 60 μmolC g^{-1} FW at the end of the night in all studies except Experiment 2, compared to a wild-type level of 14–27 μmolC g^{-1} FW (Fig. 4B). In-chamber recordings showed aberrant temperature averaging 18.5 °C in the growth chamber for this experiment alone, rather than the intended 20.5 °C. The double-mutant clock's long circadian period is known to be fully restored to wild type at 12.5 °C (Salome *et al.* 2006), hence the lower growth temperature likely weakened the effect of this temperature-conditional mutation, in this experiment. The P2011 clock model is calibrated for regulation at 21 °C and is not expected to simulate temperature-dependent effects, hence the modelling of Experiment 2 used observed rather than predicted

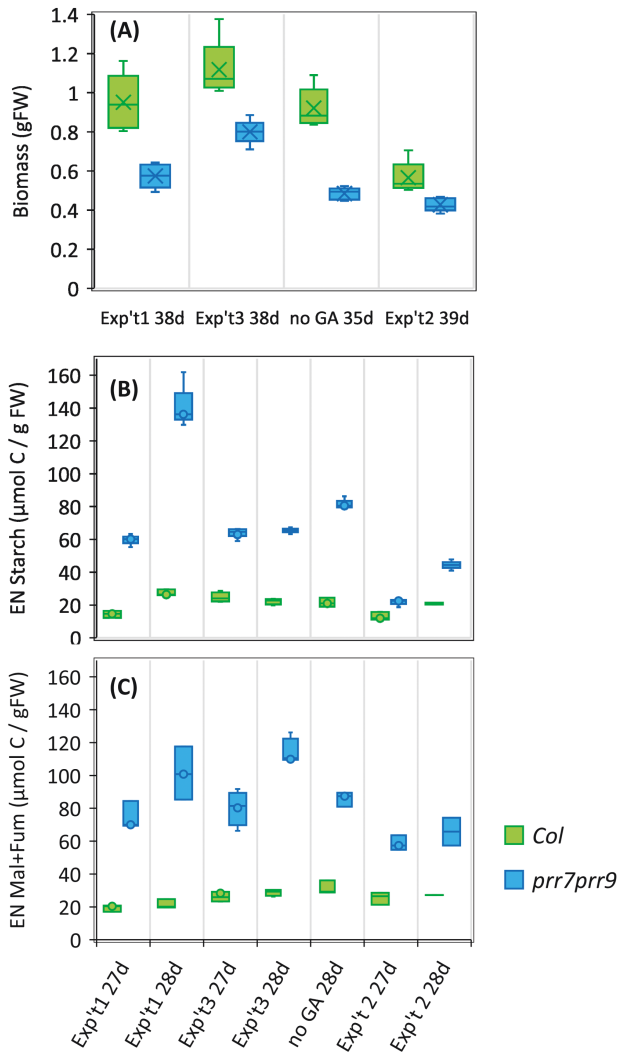

Figure 4. Replication of biomass and carbon storage traits. (A) The range of *prr7prr9* final biomass (indicated by whiskers; blue) is below the range for Col (green) in all experiments, with the smallest difference in experiment 2 (right-hand columns), at 18.5 °C rather than 20.5 °C in the other studies. Data are mean, *n* = 5, error bar = SD. Exp't 1 and 3, 38 days after sowing (38d); no GA controls, 35 days; Exp't 2, 39 days. *prr7prr9* plants also show excess levels of (B) starch and (C) malate + fumarate at the end of the night (EoN, ≡EN) in all experiments, with the starch level of *prr7prr9* plants closest to Col in experiment 2. Data are mean, *n* = 3 (Exp't 3, *n* = 4), error bar = SD (Exp't 1, 2 and 3, 27 and 28 days after sowing; no GA controls, 28 days only). Data collated from Fig. 3 and Supporting Information—Figs 9 and 11. Differences in sampling among experiments are outlined in Supporting Information.

starch degradation rates [**see Supporting Information—Section 4**; **Supporting Information—Table S1**].

These results provide a proof of concept, showing that the pervasive effects of altered circadian timing at the level of the whole plant can be understood quantitatively, in terms of the underlying biochemical and molecular mechanisms (see Discussion section). The effect of clock mutations on starch metabolism was most significant in accounting for the mutants' lower biomass, and changes in malate and fumarate levels accounted for any remaining growth defect.

3.6 Testing potential mechanisms for circadian mis-regulation of organic acid pools

We next tested several processes that might alter malate and fumarate synthesis or utilization in *prr7prr9*. The FMv2 simulations reduced malate and fumarate utilization in the *prr7prr9* mutant but we also tested the possibility of increased malate synthesis, via CO_2 fixation by PEP carboxylase. This can be measured as $^{14}CO_2$ fixation in darkness, which was very low compared with photosynthetic CO_2 assimilation (Kölling *et al.* 2015) but nevertheless measurable. Total dark CO_2 fixation was similar in the *prr7prr9* mutants and the wild type [**see Supporting Information—Fig. S10A**]. However, the distribution of labelled carbon between compound classes differed [**see Supporting Information—Fig. S10B and C**]. Most was found in water-soluble acidic compounds (i.e. organic acids derived from PEP carboxylase action) and water-soluble basic compounds (presumably amino acids produced from the organic acids). While *prr7prr9* had slightly less label in soluble compounds overall, there was more in the acidic fraction and less in the basic fraction than in the wild type. Some label was found in proteins, with the amount in *prr7prr9* (12 ± 1 %) significantly exceeding that of the wild type (7 ± 1 %) leading to a slightly higher labelling of the insoluble fraction in the mutant.

Second, altered expression of the clock-regulated, thiamine-biosynthetic gene *THIAMINE C* (*THIC*) in *prr7prr9* might alter organic acid levels, by affecting thiamine-cofactor-dependent, metabolic enzymes (Raschke *et al.* 2007; Bocobza *et al.* 2013; Rosado-Souza *et al.* 2019). Biosynthetic intermediates thiamine monophosphate and thiamine indeed accumulated at 2- to 3-fold higher levels in the *prr7prr9* mutants [**see Supporting Information—Fig. S10F and G**], though levels of THIC protein were reduced in this genotype (Supplementary Table 2 of Graf *et al.* 2017). The level of the active thiamine diphosphate (TDP) cofactor (vitamin B1) increased by less than 10 % [**see Supporting Information—Fig. S10E**], which was not statistically significant and suggested that homeostatic mechanisms were largely compensating for any circadian mis-regulation.

Third, reduced carbon demand from growth, rather than or in addition to redirected carbon supply, might promote organic acid accumulation indirectly (see Discussion section). We applied exogenous GAs to test whether stimulating growth could increase biomass in *prr7prr9*, by mobilizing the mutant's excess carbon stores into biomass. Gibberellin treatment indeed increased the biomass of both genotypes to a similar extent [**see Supporting Information—Fig. S11A**] but this was not through greater mobilization of the clock-dependent carbon pools. Gibberellin treatment had little or no effect on starch or malate levels at the end of the night (Ribeiro *et al.* 2012; **see Supporting Information—Fig. S11C–E**), and increased the fumarate level. The starch level at the end of the day was slightly reduced in GA-treated *prr7prr9* plants. To control for a direct effect of GA on the mutants' clock defect, given that the clock affects GA sensitivity (Arana *et al.* 2011), we confirmed that GA treatment did not rescue the

circadian period defect in *prr7prr9* plants tested by luciferase reporter gene imaging under constant light [**see Supporting Information—Fig. S11F**]. Thus, GA treatment likely stimulated biomass growth by a mechanism orthogonal to the growth-limiting effect of the clock mutations. Consistent with this, we found little overlap in previously tested transcriptome responses to GA treatment (Bai *et al.* 2012) and the arrhythmic *prr5prr7prr9* clock mutation (Nakamichi *et al.* 2009; **see Supporting Information—Fig. S11G**), which also accumulates malate and fumarate (Fukushima *et al.* 2009).

4. DISCUSSION

The *Arabidopsis* FMv2 builds upon the delayed gene expression patterns in *prr7prr9* double mutants to predict canonical clock phenotypes, under the standard laboratory conditions previously used to define these phenotypes. The greater hypocotyl elongation and delayed flowering time simulated in the mutants result from gene expression cascades in the S2015 submodel, which represents similar molecular processes to the clock gene circuit represented in the P2011 submodel. This aspect of the FMv2 is helpful to understand the effects of these gene expression regulators at the whole-plant scale (Krahmer *et al.* 2019). Regulatory pathways beyond the light and clockgene network could be included in future, but the earlier FMv1 model has been most used to simulate the growth of the *Arabidopsis* rosette, or the interaction of rosette development with these gene circuits. The FMv2 bridges from gene circuit dynamics not only to these developmental issues but also to carbon biomass growth, via its simple model of photosynthetic metabolism. **Supporting Information—Table S2** summarizes the predictions tested here, the gaps revealed and those that could be tested in future.

Rhythmic output from the clock gene circuit to the metabolic network, in the chloroplast, controls the simulated level of transient starch that remains at the end of the night in the FMv2. The model correctly predicted the higher starch levels observed in the *prr7prr9* mutants, due to their delayed circadian timing. The whole-plant context of the Framework Model then allowed us to test whether that metabolic change predicted an altered biomass in the mutants compared to wild-type plants. Mis-timed starch degradation largely (58–65 % of the biomass reduction in Experiments 1 and 2) or entirely (Experiment 3) accounted for the mutants' observed biomass. This result agrees with a previous conclusion (Graf *et al.* 2010) and contrasts with an earlier report that circadian mis-timing lowered photosynthetic rates (Dodd *et al.* 2005). The *prr7prr9* mutants showed no reduction in photosynthesis or chlorophyll levels in our conditions (see **Supporting Information—Fig. S5** and data shared online), though the two earlier studies used different growth conditions and clock mutants. Unused malate and fumarate accounted for the remaining biomass defect of *prr7prr9* mutants in Experiments 1 and 2. These metabolite pools had previously been linked to clock gene function by machine-learning analysis (Grzegorczyk *et al.* 2015). The same mechanisms might affect the biomass growth of arrhythmic *prr5prr7prr9* mutants, which also accumulate these organic acids (Fukushima *et al.* 2009).

The most striking metabolic effect of mis-timing in the *prr7prr9* double-mutant plants is an increased baseline starch level, rather than a slower starch degradation rate, but the models link these phenotypes parsimoniously. Consider first the *lsf1* control plants (Fig. 3E), where the mutation is assumed to reduce the relative starch degradation rate, that is, the degradation rate per unit of starch. The plant's starch metabolism in each unit of leaf area is close to a steady state, where the absolute amount of starch degraded nightly per unit leaf area equals the daily synthesis. The whole plants are not in a steady state, because their total leaf area is growing. *lsf1* does not affect photosynthesis [**see Supporting Information—Fig. S5**] or the partitioning of photosynthate into starch, so the daily starch synthesis of *lsf1* mutants per unit of leaf area is the same as in wild-type plants (Fig. 3E). To degrade that amount of starch per unit leaf area every night, the *lsf1* plants' lower relative starch degradation rate per unit of starch must be applied to a larger pool of starch than in wild-type plants. The higher 'baseline' starch level at the end of the night in *lsf1* reflects this increased starch pool. Hence, the higher baseline level follows naturally from a steady state with a slower relative starch degradation rate, in ours and similar models (Pokhilko *et al.* 2014; Seaton *et al.* 2014). The assumption of a lower relative degradation rate in *lsf1* is therefore functionally equivalent to the previous assumption of an altered 'starch set point' baseline level (Comparot-Moss *et al.* 2010; Scialdone *et al.* 2013). Only the relative starch degradation rate needs to be altered in simulations of *lsf1* [**see Supporting Information—Table S1**], in order for the FMv2 to recapitulate the observed, higher baseline starch levels (Fig. 3E). Exactly the same argument can explain the higher starch levels in the *prr7prr9* mutants. The *prr* mutations indirectly reduce the relative starch degradation rate, per unit starch, via their effects on the dynamics of the clock gene circuit.

Why then do the mutant plants have lower total biomass, if they mobilize the same absolute amount of starch each night as the wild type in each unit of leaf area (Fig. 3F)? The explanation supported by the model is that the mutant plants accumulate large, unused starch pools as well as new biomass, whereas wild-type plants use the same photoassimilate supply to produce biomass more efficiently, leaving only a minimum of carbon in starch. As the plants continue to grow, the effect on biomass is cumulative: the leaf area that is not produced on 1 day results in a penalty on the plant's total photosynthetic rate on every future day. Consistent with this mechanism, many parameter changes that reduced simulated starch levels at the end of the night also increased predicted biomass [**see Supporting Information—Fig. S7**].

The biochemical mechanisms that connect clock output to starch degradation rate remain under investigation (Smith and Zeeman 2020). Neither of the candidate biochemical mechanisms for misregulation of malate and fumarate levels that we tested (PEPC activity and TDP level; **see Supporting Information—Fig. S10**) was obviously affected in the double mutants. Firstly, subtle changes might have significant, cumulative effects on final plant biomass and yet be below the resolution of our single time point, biochemical assays. Secondly, a mathematical model cannot predict such biochemical mechanisms in much greater detail than has been tested in the available data. Including a richer model of central metabolism (Cheung *et al.* 2015) in the Framework Model could bring more of our metabolic data [**see Supporting Information—Fig. S3**] to bear on this question. Until such causal mechanisms are determined, alternative explanations remain possible.

We assume that the altered starch levels cause the biomass defect in the *lsf1* mutants, because the LSF1 protein is located in the chloroplast

and normally functions in starch degradation (Comparot-Moss *et al.* 2010; Schreier *et al.* 2019). The FMv2 simulations altered the starch levels of *prr7prr9* mutants by a very similar mechanism: removing PRR7 and PRR9 proteins from the clock submodel predicted the clock-regulated slowing of the relative starch degradation rate and smaller plants as a result (as in Fig. 3). Other models of starch dynamics have also represented a clock-regulated mechanism of this type (Scialdone *et al.* 2013; Pokhilko *et al.* 2014). However, an accurate model prediction is not a guarantee that the model is based on the correct explanation. We cannot infer the same causation as in *lsf1*, while the biochemical connection from the clock to starch regulation is unknown and cannot be directly tested in *prr7prr9*. We therefore conclude that the observed metabolic phenotypes arithmetically account for the clock mutants' biomass growth defect, and that clock-regulated starch degradation is a feasible mechanism. In this scenario, the mechanisms of malate and fumarate mis-regulation in the clock mutants are unclear, as noted above.

Alternatively or in addition, the clock might directly regulate growth rate, leading to mis-regulated growth in the mis-timed clock-mutant plants. Slower growth in the *prr7prr9* double mutants might then leave unused photoassimilate to build up in various metabolite pools, including starch, malate and fumarate. Several lines of evidence suggest that such growth regulation is possible, though its mechanism is also unknown (Massonnet *et al.* 2011; Flis *et al.* 2019; Pullen *et al.* 2019). The GA pathway was a candidate mechanism for this circadian effect; however, our limited results were not obviously consistent with GAs as the mechanism for growth mis-regulation in *prr7prr9* [**see Supporting Information—Fig. S11**]. The Framework Model could be adapted in future to distinguish these alternative directions of causation, as well as to test the mechanisms for a wide range of detailed behaviours that link the dynamics of light, circadian, metabolic and growth regulation.

Mugford *et al.* (2014) and Mengin *et al.* (2017), for example, suggest that the high sucrose observed after dawn in short photoperiods might accumulate due to the plant's observed delay in resuming growth after a long night (and similarly after other perturbations that limit night-time sugar supply; Gibon *et al.* 2004; Usadel *et al.* 2008; Moraes *et al.* 2019). This sucrose peak was proposed to increase AGPase activity allosterically [**see Supporting Information—Fig. S2A**], and the FMv2 uses this outcome as the mechanism to increase carbon partitioning to starch under short photoperiods. Mugford *et al.* also showed that *fkf1* and perhaps *gi* mutants lacked this photoperiodic adjustment of partitioning (Mugford *et al.* 2014). The FMv2 already represents the key variables required to support future studies of this mechanism.

Whole-plant models based in molecular pathways are rare, because these studies remain challenging. Firstly, they require data of many types, ideally all acquired from the same plants, with calibration data at multiple scales that allow the models to use absolute units. Secondly, any environmental regulatory mechanism, such as the circadian clock, is sensitive to the experimental conditions, which can therefore contribute to variability in the data. For example, the *prr7prr9* mutant phenotypes altered in Experiment 2, likely due to a 2 °C lower growth temperature. Thirdly, there is often a balance to be struck between the specificity of an experimental manipulation (in this case the delayed timing of *prr7prr9*) and the magnitude of its effects, where an effect close in scale to stochastic, inter-plant variation can be laborious to reproduce but a more dramatic manipulation risks causing an unknown number of indirect effects, for example, through carbon starvation. This work used broad experimental and modelling expertise, in organizations with dedicated facilities for plant systems biology, linked internationally by successive project awards [**see Supporting Information—Fig. S12**]. Accounting for the mild growth defect of *prr7prr9* via particular biochemical mechanisms was at the limit of experimental tractability in our hands, due to the challenges noted above.

The approach has not been widely applied by *Arabidopsis* researchers, so we have considered how to facilitate its adoption. Users of the earlier FMv1 have been expert modellers, for example, so there has so far been little benefit from our investment in providing full access to FMv1 in user-friendly software with a graphical interface (Chew *et al.* 2014). A simpler, online simulator is therefore provided for non-experts to run the FMv2 [**see Supporting Information—Fig. S13**]. The scope of potential, future developments is broad. High-resolution phenotyping systems might soon resolve both physiological variation among individual plants and individual-specific, micro-environmental parameters, both in controlled environments and field conditions. The FMv2 could underpin a 'digital twin' approach to simulate each plant, which is closer in outlook to personalized medicine. Extensions of the Framework Model [**see Supporting Information—Table S2**] might test other critical rhythmic functions, such as photosynthesis, and address the nutrient and water limitations that prevail in field conditions. Even in our well-watered conditions, the *prr7prr9* clock mutants had consistently lower water content than wild-type plants [**see Supporting Information—Fig. S9K**], suggesting another tractable effect that might be mediated by circadian mis-regulation of aquaporins and/or abscisic acid (Adams *et al.* 2018; Prado *et al.* 2019). Whole-organism physiology could also be understood (explained and predicted) quantitatively in other multicellular species (Le Novere 2015), for example, using clock and metabolic models in animals and humans to understand body composition (Peek *et al.* 2013).

SUPPORTING INFORMATION

The following additional information is available in the online version of this article—

Section 1. Updating the circadian clock, starch and photoperiod response models
Section 1.1 Photoperiod response model
Section 1.2 Circadian control of starch turnover
Section 2. Revision of starch synthesis
Section 3. Addition of carbon pool for malate and fumarate
Section 4. Parameter calibration
Section 5. Modelling protein synthesis, compared to literature data
Section 6. References
Table S1. Parameter and cvRMSE values for all studies and genotypes.
Table S2. Outcomes from the FMv2: predictions, gaps and future studies.
Figure S1. Simulation of clock outputs.
Figure S2. Updating the carbon dynamic model (CDM).
Figure S3. Primary metabolites for Col and *prr7prr9* mutant plants measured at the end of day and the end of night.

Figure S4. Flow diagram of parameter calibration.
Figure S5. Gas exchange measurement and leaf number of different mutants.
Figure S6. Biomass and carbon status of *prr7* mutants.
Figure S7. Parameter sensitivity overview.
Figure S8. Model sensitivity to water content parameter.
Figure S9. Repeated tests of biomass growth, starch and organic acid content.
Figure S10. Testing direct mechanisms of malate and fumarate accumulation.
Figure S11. Testing gibberellin-stimulated growth for reversal of the clock-mediated carbon accumulation.
Figure S12. Provenance of the *Arabidopsis* Framework Model version 2 (FMv2).
Figure S13. Online simulator for the *Arabidopsis* Framework Model version 2 (FMv2).

ACKNOWLEDGEMENTS

A.J.M. dedicates his contribution to the memory of Prof. J. Andrew Bangham, who saw most clearly the potential for the 'digital cell, weed and worm', and of Prof. Tom ap Rees, mentor to S.C.Z., A.M.S., M.S. and A.J.M. For the purpose of open access, the authors have applied a CC-BY public copyright licence to any Author Accepted Manuscript version arising from this submission.

SOURCES OF FUNDING

Supported by European Commission FP7 collaborative project TiMet (contract 245143) to several authors, BBSRC FLIP fellowship BB/M017605 to A.H. and a BBSRC Institute Strategic Programme Grant BB/J004561/1 to the John Innes Centre. Financial support is gratefully acknowledged from the Swiss National Science Foundation (grant 31003A_162555) and the University of Geneva to T.B.F., from the Zürich–Basel Plant Science Centre Plant Fellows Programme (Marie Skłodowska-Curie Action Grant GA-2010-267243) and ETH Zurich to G.M.G. and S.C.Z.

CONFLICT OF INTEREST

None declared.

CONTRIBUTIONS BY THE AUTHORS

Y.H.C., A.M.S., M.S. and A.J.M. designed the study. Y.H.C., V.M., A.F., S.T.M., A.M.S. and M.S. performed the main experiments and analysed the experimental data. Y.H.C. and D.D.S. performed the modelling and analysed the simulation results. D.D.S., M.M., T.B.F., G.M.G. and S.C.Z. designed, performed and analysed follow-up studies. A.H. tested models and developed the online simulator. Y.H.C., D.D.S. and A.J.M. wrote the paper with input from all authors.

DATA AVAILABILITY

The data are shared collectively as a static Snapshot, formatted as a Research Object and structured according to the standard ISA hierarchy, on FAIRDOMHub.org (doi: 10.15490/fairdomhub.1.investigation.123.1), on the Zenodo repository (doi: 10.5281/zenodo.6536645) and on the University of Edinburgh DataShare (https://doi.org/10.7488/ds/3453). Within the Snapshot, the model is linked from the GitHub repository. We recommend consulting the live, updatable resource, which is easiest to use: https://fairdomhub.org/investigations/123. The Open Data include results that are not analysed here, including metabolite levels at 21 days after sowing, and results from the *pgm* starch mutant in Experiments 2 and 3 and the *lhy;cca1* clock double mutant in Experiment 3 and the dark assimilation study. The data should be cited using the relevant doi, for example, as: Chew, Y.H. et al. (2022). Prediction and analysis of phenotypes in the *Arabidopsis* clock-mutant *prr7prr9* using the Framework Model v2 (FMv2) [Data set]. Zenodo. https://doi.org/10.5281/zenodo.6536645. The luciferase reporter gene assays for circadian period of Col-0 and *prr7prr9* seedlings, with and without exogenous GA, are available from the BioDare repository (Moore *et al.* 2014) as BioDare experiment ID 3838: choose https://biodare.ed.ac.uk/experiment ('Browse Public Resources' on the Login screen), then https://biodare.ed.ac.uk/robust/ShowExperiment.action?experimentId=3838, 'Effects of GA on clock in WT and prr9prr7'. Raw and processed data, metadata, period analysis and summary statistics are available. A simple, online simulator allows non-experts to run the FMv2 for wild type and *prr7prr9* in multiple conditions, with a public, web browser interface at http://turnip.bio.ed.ac.uk/fm/ [**see Supporting Information—Fig. S13**].

LITERATURE CITED

Adams S, Grundy J, Veflingstad SR, Dyer NP, Hannah MA, Ott S, Carré IA. 2018. Circadian control of abscisic acid biosynthesis and signalling pathways revealed by genome-wide analysis of LHY binding targets. *New Phytologist* **220**:893–907.

Arana MV, Marin-de la Rosa N, Maloof JN, Blazquez MA, Alabadi D. 2011. Circadian oscillation of gibberellin signaling in *Arabidopsis*. *Proceedings of the National Academy of Sciences of the United States of America* **108**:9292–9297.

Arrivault S, Guenther M, Ivakov A, Feil R, Vosloh D, van Dongen JT, Sulpice R, Stitt M. 2009. Use of reverse-phase liquid chromatography, linked to tandem mass spectrometry, to profile the Calvin cycle and other metabolic intermediates in *Arabidopsis* rosettes at different carbon dioxide concentrations. *Plant Journal* **59**:826–839.

Bai MY, Shang JX, Oh E, Fan M, Bai Y, Zentella R, Sun TP, Wang ZY. 2012. Brassinosteroid, gibberellin and phytochrome impinge on a common transcription module in *Arabidopsis*. *Nature Cell Biology* **14**:810–817.

Band LR, Wells DM, Fozard JA, Ghetiu T, French AP, Pound MP, Wilson MH, Yu L, Li W, Hijazi HI, Oh J, Pearce SP, Perez-Amador MA, Yun J, Kramer E, Alonso JM, Godin C, Vernoux T, Hodgman TC, Pridmore TP, Swarup R, King JR, Bennett MJ. 2014. Systems analysis of auxin transport in the *Arabidopsis* root apex. *Plant Cell* **26**:862–875.

Bendix C, Marshall CM, Harmon FG. 2015. Circadian clock genes universally control key agricultural traits. *Molecular Plant* **8**:1135–1152.

Bocobza SE, Malitsky S, Araujo WL, Nunes-Nesi A, Meir S, Shapira M, Fernie AR, Aharoni A. 2013. Orchestration of thiamin biosynthesis and central metabolism by combined action of the thiamin pyrophosphate riboswitch and the circadian clock in *Arabidopsis*. *Plant Cell* **25**:288–307.

Cheung CY, Ratcliffe RG, Sweetlove LJ. 2015. A method of accounting for enzyme costs in flux balance analysis reveals alternative pathways and metabolite stores in an illuminated *Arabidopsis* leaf. *Plant Physiology* **169**:1671–1682.

Chew YH, Wenden B, Flis A, Mengin V, Taylor J, Davey CL, Tindal C, Thomas H, Ougham HJ, de Reffye P, Stitt M, Williams M, Muetzelfeldt R, Halliday KJ, Millar AJ. 2014. Multiscale digital *Arabidopsis* predicts individual organ and whole-organism growth. *Proceedings of the National Academy of Sciences of the United States of America* **111**:E4127–E4136.

Chew YH, Wilczek AM, Williams M, Welch SM, Schmitt J, Halliday KJ. 2012. An augmented *Arabidopsis* phenology model reveals seasonal temperature control of flowering time. *New Phytologist* **194**:654–665.

Christophe A, Letort V, Hummel I, Cournede PH, de Reffye, P, Lecoeur J. 2008. A model-based analysis of the dynamics of carbon balance at the whole-plant level in *Arabidopsis thaliana*. *Functional Plant Biology* **35**:1147–1162.

Clark TJ, Guo L, Morgan J, Schwender J. 2020. Modeling plant metabolism: from network reconstruction to mechanistic models. *Annual Review of Plant Biology* **71**:303–326.

Comparot-Moss S, Kotting O, Stettler M, Edner C, Graf A, Weise SE, Streb S, Lue WL, MacLean D, Mahlow S, Ritte G, Steup M, Chen J, Zeeman SC, Smith AM. 2010. A putative phosphatase, LSF1, is required for normal starch turnover in *Arabidopsis* leaves. *Plant Physiology* **152**:685–697.

De Caluwé J, Xiao Q, Hermans C, Verbruggen N, Leloup J-C, Gonze D. 2016. A compact model for the complex plant circadian clock. *Frontiers in Plant Science* **7**:74.

Dodd AN, Salathia N, Hall A, Kevei E, Toth R, Nagy F, Hibberd JM, Millar AJ, Webb AA. 2005. Plant circadian clocks increase photosynthesis, growth, survival, and competitive advantage. *Science* **309**:630–633.

Flis A, Fernandez AP, Zielinski T, Mengin V, Sulpice R, Stratford K, Hume A, Pokhilko A, Southern MM, Seaton DD, McWatters HG, Stitt M, Halliday KJ, Millar AJ. 2015. Defining the robust behaviour of the plant clock gene circuit with absolute RNA time series and open infrastructure. *Open Biology* **5**:150042.

Flis A, Mengin V, Ivakov AA, Mugford ST, Hubberten HM, Encke B, Krohn N, Hohne M, Feil R, Hoefgen R, Lunn JE, Millar AJ, Smith AM, Sulpice R, Stitt M. 2019. Multiple circadian clock outputs regulate diel turnover of carbon and nitrogen reserves. *Plant Cell and Environment* **42**:549–573.

Fogelmark K, Troein C. 2014. Rethinking transcriptional activation in the *Arabidopsis* circadian clock. *PLoS Computational Biology* **10**:e1003705.

Fukushima A, Kusano M, Nakamichi N, Kobayashi M, Hayashi N, Sakakibara H, Mizuno T, Saito K. 2009. Impact of clock-associated *Arabidopsis* pseudo-response regulators in metabolic coordination. *Proceedings of the National Academy of Sciences of the United States of America* **106**:7251–7256.

Gibon Y, Blasing OE, Palacios-Rojas N, Pankovic D, Hendriks JH, Fisahn J, Hohne M, Gunther M, Stitt M. 2004. Adjustment of diurnal starch turnover to short days: depletion of sugar during the night leads to a temporary inhibition of carbohydrate utilization, accumulation of sugars and post-translational activation of ADP-glucose pyrophosphorylase in the following light period. *Plant Journal* **39**:847–862.

Graf A, Coman D, Uhrig RG, Walsh S, Flis A, Stitt M, Gruissem W. 2017. Parallel analysis of *Arabidopsis* circadian clock mutants reveals different scales of transcriptome and proteome regulation. *Open Biology* **7**:160333.

Graf A, Schlereth A, Stitt M, Smith AM. 2010. Circadian control of carbohydrate availability for growth in *Arabidopsis* plants at night. *Proceedings of the National Academy of Sciences of the United States of America* **107**:9458–9463.

Grafahrend-Belau E, Junker A, Eschenroder A, Muller J, Schreiber F, Junker BH. 2013. Multiscale metabolic modeling: dynamic flux balance analysis on a whole-plant scale. *Plant Physiology* **163**:637–647.

Green RM, Tingay S, Wang ZY, Tobin EM. 2002. Circadian rhythms confer a higher level of fitness to *Arabidopsis* plants. *Plant Physiology* **129**:576–584.

Grzegorczyk M, Aderhold A, Husmeier D. 2015. Inferring bi-directional interactions between circadian clock genes and metabolism with model ensembles. *Statistical Applications in Genetics and Molecular Biology* **14**:143–167.

Hammer G, Messina C, Wu A, Cooper M. 2019. Biological reality and parsimony in crop models—why we need both in crop improvement!. *in silico Plants* **1**:diz010; doi:10.1093/insilicoplants/diz010.

Haydon MJ, Mielczarek O, Robertson FC, Hubbard KE, Webb AA. 2013. Photosynthetic entrainment of the *Arabidopsis thaliana* circadian clock. *Nature* **502**:689–692.

Ishihara H, Alseekh S, Feil R, Perera P, George GM, Niedzwiecki P, Arrivault S, Zeeman SC, Fernie AR, Lunn JE, Smith AM, Stitt M. 2022. Rising rates of starch degradation during daytime and trehalose 6-phosphate optimize carbon availability. *Plant Physiology*. doi:10.1093/plphys/kiac162.

Ishihara H, Obata T, Sulpice R, Fernie AR, Stitt M. 2015. Quantifying protein synthesis and degradation in *Arabidopsis* by dynamic (CO2)-C-13 labeling and analysis of enrichment in individual amino acids in their free pools and in protein (vol 168, pg 74, 2015). *Plant Physiology* **168**:741179–741193.

Kinmonth-Schultz HA, MacEwen MJS, Seaton DD, Millar AJ, Imaizumi T, Kim S-H. 2019. An explanatory model of temperature influence on flowering through whole-plant accumulation of FLOWERING LOCUS T in *Arabidopsis thaliana*. *in silico Plants* **1**:diz006; doi:10.1093/insilicoplants/diz006.

Kölling K, Muller A, Flutsch P, Zeeman SC. 2013. A device for single leaf labelling with CO_2 isotopes to study carbon allocation and partitioning in *Arabidopsis thaliana*. *Plant Methods* **9**:45.

Kölling K, Thalmann M, Muller A, Jenny C, Zeeman SC. 2015. Carbon partitioning in *Arabidopsis thaliana* is a dynamic process controlled by the plants metabolic status and its circadian clock. *Plant Cell and Environment*. doi:10.1111/pce.12512.

Krahmer J, Abbas A, Mengin V, Ishihara H, Romanowski A, Furniss JJ, Moraes TA, Krohn N, Annunziata MG, Feil R, Alseekh S, Obata T, Fernie AR, Stitt M, Halliday KJ. 2021. Phytochromes control metabolic flux, and their action at the seedling stage determines adult plant biomass. *Journal of Experimental Botany* **72**:3263–3278.

Krahmer J, Goralogia GS, Kubota A, Zardilis A, Johnson RS, Song YH, MacCoss MJ, Bihan TL, Halliday KJ, Imaizumi T, Millar AJ. 2019. Time-resolved interaction proteomics of the GIGANTEA protein under diurnal cycles in *Arabidopsis*. *FEBS Letters* **593**:319–338.

Kuhlman SJ, Craig LM, Duffy JF. 2018. Introduction to chronobiology. *Cold Spring Harbor Perspectives in Biology* **10**:a033613.

Le Novere N. 2015. Quantitative and logic modelling of molecular and gene networks. *Nature Reviews Genetics* **16**:146–158.

Locke JC, Southern MM, Kozma-Bognar L, Hibberd V, Brown PE, Turner MS, Millar AJ. 2005. Extension of a genetic network model by iterative experimentation and mathematical analysis. *Molecular Systems Biology* **1**:2005–0013.

Massonnet C, Tisne S, Radziejwoski A, Vile D, De Veylder L, Dauzat M, Granier C. 2011. New insights into the control of endoreduplication: endoreduplication could be driven by organ growth in *Arabidopsis* leaves. *Plant Physiology* **157**:2044–2055.

Matthews ML, Marshall-Colon A. 2021. Multiscale plant modeling: from genome to phenome and beyond. *Emerging Topics in Life Sciences* doi:10.1042/ETLS20200276.

Mengin V, Pyl ET, Alexandre Moraes T, Sulpice R, Krohn N, Encke B, Stitt M. 2017. Photosynthate partitioning to starch in *Arabidopsis thaliana* is insensitive to light intensity but sensitive to photoperiod due to a restriction on growth in the light in short photoperiods. *Plant Cell and Environment* **40**:2608–2627.

Millar AJ. 2016. The intracellular dynamics of circadian clocks reach for the light of ecology and evolution. *Annual Review of Plant Biology* **67**:595–618.

Moore A, Zielinski T, Millar AJ. 2014. Online period estimation and determination of rhythmicity in circadian data, using the BioDare data infrastructure. *Methods in Molecular Biology* **1158**:13–44.

Moraes TA, Mengin V, Annunziata MG, Encke B, Krohn N, Hohne M, Stitt M. 2019. Response of the circadian clock and diel starch turnover to one day of low light or low CO_2. *Plant Physiology* **179**:1457–1478.

Moulin M, Nguyen GT, Scaife MA, Smith AG, Fitzpatrick TB. 2013. Analysis of *Chlamydomonas* thiamin metabolism in vivo reveals riboswitch plasticity. *Proceedings of the National Academy of Sciences of the United States of America* **110**:14622–14627.

Mugford ST, Fernandez O, Brinton J, Flis A, Krohn N, Encke B, Feil R, Sulpice R, Lunn JE, Stitt M, Smith AM. 2014. Regulatory properties of ADP glucose pyrophosphorylase are required for adjustment of leaf starch synthesis in different photoperiods. *Plant Physiology* **166**:1733–1747.

Muller NA, Wijnen CL, Srinivasan A, Ryngajllo M, Ofner I, Lin T, Ranjan A, West D, Maloof JN, Sinha NR, Huang S, Zamir D, Jimenez-Gomez JM. 2015. Domestication selected for deceleration of the circadian clock in cultivated tomato. *Nature Genetics*. doi:10.1038/ng.3447.

Nakamichi N, Kiba T, Henriques R, Mizuno T, Chua NH, Sakakibara H. 2010. PSEUDO-RESPONSE REGULATORS 9, 7, and 5 are transcriptional repressors in the *Arabidopsis* circadian clock. *Plant Cell* **22**:594–605.

Nakamichi N, Kita M, Niinuma K, Ito S, Yamashino T, Mizoguchi T, Mizuno T. 2007. *Arabidopsis* clock-associated pseudo-response regulators PRR9, PRR7 and PRR5 coordinately and positively regulate flowering time through the canonical CONSTANS-dependent photoperiodic pathway. *Plant and Cell Physiology* **48**:822–832.

Nakamichi N, Kusano M, Fukushima A, Kita M, Ito S, Yamashino T, Saito K, Sakakibara H, Mizuno T. 2009. Transcript profiling of an *Arabidopsis* PSEUDO RESPONSE REGULATOR arrhythmic triple mutant reveals a role for the circadian clock in cold stress response. *Plant and Cell Physiology* **50**:447–462.

Niwa Y, Yamashino T, Mizuno T. 2009. The circadian clock regulates the photoperiodic response of hypocotyl elongation through a coincidence mechanism in *Arabidopsis thaliana*. *Plant and Cell Physiology* **50**:838–854.

Ouyang Y, Andersson CR, Kondo T, Golden SS, Johnson CH. 1998. Resonating circadian clocks enhance fitness in cyanobacteria. *Proceedings of the National Academy of Sciences of the United States of America* **95**:8660–8664.

Paschos GK, Baggs JE, Hogenesch JB, FitzGerald GA. 2010. The role of clock genes in pharmacology. *Annual Review of Pharmacology and Toxicology* **50**:187–214.

Pay ML, Kim DW, Somers DE, Kim JK, Foo M. 2022. Modelling of plant circadian clock for characterizing hypocotyl growth under different light quality conditions. *in silico Plants* **4**:diac001; doi:10.1093/insilicoplants/diac001.

Peek CB, Affinati AH, Ramsey KM, Kuo HY, Yu W, Sena LA, Ilkayeva O, Marcheva B, Kobayashi Y, Omura C, Levine DC, Bacsik DJ, Gius D, Newgard CB, Goetzman E, Chandel NS, Denu JM, Mrksich M, Bass J. 2013. Circadian clock NAD^+ cycle drives mitochondrial oxidative metabolism in mice. *Science* **342**:1243417.

Pokhilko A, Fernandez AP, Edwards KD, Southern MM, Halliday KJ, Millar AJ. 2012. The clock gene circuit in *Arabidopsis* includes a repressilator with additional feedback loops. *Molecular Systems Biology* **8**:574.

Pokhilko A, Flis A, Sulpice R, Stitt M, Ebenhoh O. 2014. Adjustment of carbon fluxes to light conditions regulates the daily turnover of starch in plants: a computational model. *Molecular Biosystems* **10**:613–627.

Prado K, Cotelle V, Li G, Bellati J, Tang N, Tournaire-Roux C, Martinière A, Santoni V, Maurel C. 2019. Oscillating aquaporin phosphorylation and 14-3-3 proteins mediate the circadian regulation of leaf hydraulics. *Plant Cell* **31**:417–429.

Pullen N, Zhang N, Dobon Alonso A, Penfield S. 2019. Growth rate regulation is associated with developmental modification of source efficiency. *Nature Plants* **5**:148–152.

Pyl ET, Piques M, Ivakov A, Schulze W, Ishihara H, Stitt M, Sulpice R. 2012. Metabolism and growth in *Arabidopsis* depend on the daytime temperature but are temperature-compensated against cool nights. *Plant Cell* **24**:2443–2469.

Quick P, Siegl G, Neuhaus E, Feil R, Stitt M. 1989. Short-term water stress leads to a stimulation of sucrose synthesis by activating sucrose-phosphate synthase. *Planta* **177**:535–546.

Raschke M, Burkle L, Muller N, Nunes-Nesi A, Fernie AR, Arigoni D, Amrhein N, Fitzpatrick TB. 2007. Vitamin B1 biosynthesis in plants requires the essential iron sulfur cluster protein, THIC. *Proceedings of the National Academy of Sciences of the United States of America* **104**:19637–19642.

Rasse DP, Tocquin P. 2006. Leaf carbohydrate controls over *Arabidopsis* growth and response to elevated CO_2: an experimentally based model. *New Phytologist* **172**:500–513.

Ribeiro DM, Araujo WL, Fernie AR, Schippers JH, Mueller-Roeber B. 2012. Action of gibberellins on growth and metabolism of *Arabidopsis* plants associated with high concentration of carbon dioxide. *Plant Physiology* **160**:1781–1794.

Rosado-Souza L, Proost S, Moulin M, Bergmann S, Bocobza SE, Aharoni A, Fitzpatrick TB, Mutwil M, Fernie AR, Obata T. 2019. Appropriate thiamin pyrophosphate levels are required for acclimation to changes in photoperiod. *Plant Physiology* **180**:185–197.

Salazar JD, Saithong T, Brown PE, Foreman J, Locke JC, Halliday KJ, Carre IA, Rand DA, Millar AJ. 2009. Prediction of photoperiodic regulators from quantitative gene circuit models. *Cell* **139**:1170–1179.

Salome PA, McClung CR. 2005. PSEUDO-RESPONSE REGULATOR 7 and 9 are partially redundant genes essential for the temperature responsiveness of the *Arabidopsis* circadian clock. *Plant Cell* **17**:791–803.

Salome PA, To JP, Kieber JJ, McClung CR. 2006. *Arabidopsis* response regulators ARR3 and ARR4 play cytokinin-independent roles in the control of circadian period. *Plant Cell* **18**:55–69.

Schneider CA, Rasband WS, Eliceiri KW. 2012. NIH Image to ImageJ: 25 years of image analysis. *Nature Methods* **9**:671–675.

Schreier TB, Umhang M, Lee SK, Lue WL, Shen Z, Silver D, Graf A, Muller A, Eicke S, Stadler-Waibel M, Seung D, Bischof S, Briggs SP, Kotting O, Moorhead GBG, Chen J, Zeeman SC. 2019. LIKE SEX4 1 acts as a beta-amylase-binding scaffold on starch granules during starch degradation. *Plant Cell* **31**:2169–2186.

Scialdone A, Mugford ST, Feike D, Skeffington A, Borrill P, Graf A, Smith AM, Howard M. 2013. *Arabidopsis* plants perform arithmetic division to prevent starvation at night. *Elife* **2**:e00669.

Seaton DD, Ebenhoh O, Millar AJ, Pokhilko A. 2014. Regulatory principles and experimental approaches to the circadian control of starch turnover. *Journal of the Royal Society Interface* **11**:20130979.

Seaton DD, Graf A, Baerenfaller K, Stitt M, Millar AJ, Gruissem W. 2018. Photoperiodic control of the *Arabidopsis* proteome reveals a translational coincidence mechanism. *Molecular Systems Biology* **14**:e7962.

Seaton DD, Smith RW, Song YH, MacGregor DR, Stewart K, Steel G, Foreman J, Penfield S, Imaizumi T, Millar AJ, Halliday KJ. 2015. Linked circadian outputs control elongation growth and flowering in response to photoperiod and temperature. *Molecular Systems Biology* **11**:776.

Seki M, Ohara T, Hearn TJ, Frank A, da Silva VCH, Caldana C, Webb AAR, Satake A. 2017. Adjustment of the *Arabidopsis* circadian oscillator by sugar signalling dictates the regulation of starch metabolism. *Scientific Reports* **7**:8305.

Smith AM, Zeeman SC. 2020. Starch: a flexible, adaptable carbon store coupled to plant growth. *Annual Review of Plant Biology* **71**:217–245.

Sulpice R, Flis A, Ivakov AA, Apelt F, Krohn N, Encke B, Abel C, Feil R, Lunn JE, Stitt M. 2014. *Arabidopsis* coordinates the diurnal regulation of carbon allocation and growth across a wide range of photoperiods. *Molecular Plant* **7**:137–155.

Urquiza-García U, Millar AJ. 2021. Testing the inferred transcription rates of a dynamic, gene network model in absolute units. *in silico Plants* **3**:diab022; doi:10.1093/insilicoplants/diab022.

Usadel B, Blasing OE, Gibon Y, Poree F, Hohne M, Gunter M, Trethewey R, Kamlage B, Poorter H, Stitt M. 2008. Multilevel genomic analysis of the response of transcripts, enzyme activities and metabolites in *Arabidopsis* rosettes to a progressive decrease of temperature in the non-freezing range. *Plant Cell and Environment* **31**:518–547.

von Dassow G, Meir E, Munro EM, Odell GM. 2000. The segment polarity network is a robust developmental module. *Nature* **406**:188–192.

Welch SM, Dong ZS, Roe JL, Das S. 2005. Flowering time control: gene network modelling and the link to quantitative genetics. *Australian Journal of Agricultural Research* **56**:919–936.

Wilczek AM, Roe JL, Knapp MC, Cooper MD, Lopez-Gallego C, Martin LJ, Muir CD, Sim S, Walker A, Anderson J, Egan JF, Moyers BT, Petipas R, Giakountis A, Charbit E, Coupland G, Welch SM, Schmitt J. 2009. Effects of genetic perturbation on seasonal life history plasticity. *Science* **323**:930–934.

Zardilis A, Hume A, Millar AJ. 2019. A multi-model framework for the *Arabidopsis* life cycle. *Journal of Experimental Botany* **70**:2463–2477.

Zell MB, Fahnenstich H, Maier A, Saigo M, Voznesenskaya EV, Edwards GE, Andreo C, Schleifenbaum F, Zell C, Drincovich MF, Maurino VG. 2010. Analysis of *Arabidopsis* with highly reduced levels of malate and fumarate sheds light on the role of these organic acids as storage carbon molecules. *Plant Physiology* **152**:1251–1262.